ORIGINAL RESEARCH

Human Rhinovirus Infection of the Respiratory Tract Affects Sphingolipid Synthesis

Emily Wasserman[1], Rika Gomi[1], Anurag Sharma[1], Seunghee Hong[2], Rohan Bareja[3], Jinghua Gu[2], Uthra Balaji[2], Arul Veerappan[4], Benjamin I. Kim[5], Wenzhu Wu[1], Andrea Heras[1], Jose Perez-Zoghbi[6], Biin Sung[1], Seyni Gueye-Ndiaye[1], Tilla S. Worgall[5], and Stefan Worgall[1,2,7]

[1]Department of Pediatrics, [2]Drukier Institute for Children's Health, [3]Englaender Institute for Precision Medicine, [4]Department of Physiology, and [7]Department of Genetic Medicine, Weill Cornell Medicine, New York, New York; and [5]Department of Pathology and Cell Biology, and [6]Department of Anesthesiology, Columbia University, New York, New York

ORCID ID: 0000-0003-3700-8375 (E.W.).

Abstract

The 17q21 asthma susceptibility locus includes asthma risk alleles associated with decreased sphingolipid synthesis, likely resulting from increased expression of ORMDL3. ORMDL3 inhibits serine-palmitoyl transferase (SPT), the rate-limiting enzyme of *de novo* sphingolipid synthesis. There is evidence that decreased sphingolipid synthesis is critical to asthma pathogenesis. Children with asthma and 17q21 asthma risk alleles display decreased sphingolipid synthesis in blood cells. Reduced SPT activity results in airway hyperreactivity, a hallmark feature of asthma. 17q21 asthma risk alleles are also linked to childhood infections with human rhinovirus (RV). This study evaluates the interaction of RV with the *de novo* sphingolipid synthesis pathway, and the alterative effects of concurrent SPT inhibition in SPT-deficient mice and human airway epithelial cells. In mice, RV infection shifted lung sphingolipid synthesis gene expression to a pattern that resembles genetic SPT deficiency, including decreased expression of Sptssa, a small SPT subunit. This pattern was pronounced in lung epithelial cellular adhesion molecule ($EpCAM^+$) cells and reproduced in human bronchial epithelial cells. RV did not affect Sptssa expression in lung $CD45^+$ immune cells. RV increased sphingolipids unique to the *de novo* synthesis pathway in mouse lung and human airway epithelial cells. Interestingly, these *de novo* sphingolipid species were reduced in the blood of RV-infected wild-type mice. RV exacerbated SPT deficiency–associated airway hyperreactivity. Airway inflammation was similar in RV-infected wild-type and SPT-deficient mice. This study reveals the effects of RV infection on the *de novo* sphingolipid synthesis pathway, elucidating a potential mechanistic link between 17q21 asthma risk alleles and rhinoviral infection.

Keywords: asthma; 17q21; rhinovirus; sphingolipids; early childhood wheeze

Clinical Relevance

We show that rhinovirus infection induces airway hyperreactivity while shifting *de novo* sphingolipid synthesis gene expression and metabolism to a pattern that resembles genetic sphingolipid deficiency. Overall, our data supports the concept of *de novo* sphingolipids as a critical connection between the 17q21 asthma susceptibility locus, rhinovirus infection, and childhood asthma. Our findings will impact evolving research into asthma development and rhinovirus-induced asthma exacerbations.

(Received in original form October 8, 2021; accepted in final form December 1, 2021)

Supported by the National Institute of Allergy and Infectious Diseases grant R21/AI140724-01 (S.W.) and the generous support of Ronay Menschel, Christine and Pasco Alfaro, and Joanna Weiss. E.W. was supported by the National Center for Advancing Translational Sciences of the NIH (KL2/TR0002385-01).

Author Contributions: E.W., R.G., A.S., A.V., A.H., J.P.-Z., T.S.W., and S.W. designed and performed the research. E.W., R.G., S.H., R.B., J.G., U.B., B.I.K., W.W., B.S., S.G.-N., T.S.W., and S.W. analyzed and interpreted the data. E.W., R.G., and S.W. wrote, revised, and approved the final version to be published.

Correspondence and requests for reprints should be addressed to Stefan Worgall, M.D., Ph.D., Department of Pediatrics, Weill Cornell Medicine, 413 East 69th Street, Room 1200, New York, NY 10021. E-mail: stw2006@med.cornell.edu.

This article has a data supplement, which is accessible from this issue's table of contents at www.atsjournals.org.

Am J Respir Cell Mol Biol Vol 66, Iss 3, pp 302–311, March 2022

Originally Published in Press as DOI: 10.1165/rcmb.2021-0443OC on December 1, 2021
Internet address: www.atsjournals.org

The 17q21 polymorphisms reproducibly linked to childhood asthma are also associated with increased expression of ORMDL3 (1–6). ORMDL3 inhibits serine-palmitoyl transferase (SPT), the rate-limiting enzyme in *de novo* sphingolipid synthesis, causing a decrease in the concentrations of sphingolipid species, including ceramides and sphingosine-1-phosphate (S1P) (7–11). ORMDL3-overexpressing mice demonstrate an asthma phenotype and decreased sphingolipid concentrations, whereas knockdown of ORMDL3 in lung epithelial cells leads to increased concentrations of ceramides and S1P (10, 12–14).

Decreased *de novo* sphingolipid synthesis is further functionally linked to asthmatic airway hyperreactivity. Inhibition of SPT increases airway smooth muscle contractility in tracheal rings from nonsensitized mice and humans (15) and allergen-sensitized mice (10, 16). There is growing evidence that *de novo* sphingolipid synthesis is decreased in children with asthma. Children with asthma and 17q21 asthma risk alleles demonstrate lower sphingolipid concentrations in blood and decreased *de novo* synthesis in peripheral blood mononuclear cells (17). In other asthma cohorts, early childhood plasma S1P, a sphingolipid that is exclusively generated by *de novo* synthesis, was inversely correlated with airway resistance later in life (18). Besides its regulatory effects on sphingolipid synthesis, ORMDL3 also regulates the unfolded protein response (UPR), a pathway linked to mucus hypersecretion and dysregulation of the airway immune response (13, 19).

Asthma exacerbations are periods of airway hyperreactivity, airway inflammation, and increased mucus production, in response to stimuli (20). Rhinovirus (RV) is the most common trigger of asthma exacerbations. Analyses of large pediatric asthma cohorts show the relationship between 17q21 asthma risk alleles and childhood asthma is strengthened by an episode of early life, RV-induced wheeze. This finding was specific to RV and not seen with respiratory syncytial virus, another common cause of severe lower respiratory infection in infants and children (21, 22). RV infection increases ceramide sphingolipids in epithelial cells (23), but the relationship between *de novo* synthesis and RV is unknown. Silencing of ORMDL3 in airway epithelial cells increases *de novo* sphingolipid synthesis and decreases expression of ICAM-1, the receptor for the majority of RV strains (24). Inhibition of SPT also enhances RV replication in HeLa cells (25). These findings suggest a critical interplay between RV and sphingolipid synthesis.

Here we detail the effects of RV infection on cellular sphingolipid synthesis both in lung and blood. We demonstrate that RV changes lung *de novo* sphingolipid synthesis gene expression in a pattern that resembles SPT inhibition. These gene expression changes were mirrored by decreased *de novo* sphingolipid species in the blood but contrasted with concurrent increases in sphingolipids in lung and lung epithelial cells. These findings suggest a central role for RV–sphingolipid interaction in the pathogenesis of asthma.

The accession number for the RNA sequencing data reported in this paper is National Center for Biotechnology Information Gene Expression Omnibus GSE189056 (https://www.ncbi.nlm.nih.gov/geo/query/acc.cgi?acc=GSE189056)

Methods

For detailed methods regarding RNA sequencing, sphingolipid quantification using high performed liquid chromatography with tandem mass spectrometry (HPLC-MS/MS), quantitative real-time PCR, immunostaining, and evaluation of airway contractility, please *see* the data supplement.

Preparation and RV Infection of Sphingolipid Deficient Mice

Heterozygous SPT-deficient mice, Sptlc2$^{+/-}$ (SPT) or Sptlc2$^{+/+}$ controls (Co), provided by Xian-Cheng Jiang, State University of New York Downstate Medical Center, were bred and identified by genotyping as described (26). All experiments included sex- and age-matched SPT and Co littermates between 8 and 12 weeks of age unless otherwise indicated. No mice were excluded from analyses unless indicated. All mouse experiments were approved by and performed under the Institutional Animal Care and Use Committee guidelines at Weill Cornell Medicine.

Lungs from Co, SPT, Co + RV, and SPT + RV mice were harvested 24 hours after intranasal inoculation with RV1B (5×10^6 $TCID_{50}$) or mock infection. Lung tissue was finely minced with scissors and divided for single-cell suspension or homogenization with steel beads. To prepare a single-cell suspension, minced tissue was digested using collagenase A (2 g/ml), DNase1 (0.2 g/ml), and dispase II (2 g/ml) (Roche) at 37°C for 30 minutes, filtered (40-μm filter) and incubated with ACK Lysis Buffer (Gibco) for lysis of red blood cells.

Rhinovirus

Human type A RV strains, RV1B (ATCC VR-1645) and RV16 (ATCC VR-283), were propagated in H1-HeLa cells (ATCC CRL-1958) and purified from cell lysates as per established protocols (*see* the data supplement (27). For *in vivo* infection, RV1B (5×10^6 $TCID_{50}$) was administered intranasally to SPT and Co mice. Uninfected Co and SPT mice received equal volumes of mock-infected H1-HeLa cell lysate. For *in vitro* infection, RV16 (1×10^6 $TCID_{50}$) diluted in 50 μl minimal essential media (MEM, ThermoFisher) was added to the apical surface of differentiated human bronchial epithelial cells grown in air–liquid interface (ALI). Cells were incubated with infectious media at 33°C for 1 hour, and incubation continued for an additional 24 hours.

Human Bronchial Epithelial Cells

The human bronchial epithelial cell line BCi-NS1.1, provided by R. G. Crystal, Weill Cornell Medicine, was differentiated in ALI as per previously described protocols (28). In brief, cells were expanded in PneumaCult-Ex Plus Complete medium (STEMCELL Technologies) and then seeded onto 6.5 mm Transwell (Corning) inserts at a density of 1.5×10^5 cells/well. Cells were grown to confluency to establish ALI and then airlifted and maintained in PneumaCult-Ex Plus Maintenance medium.

Statistics

All data are expressed as means ± SEM. For mice experiments, the *n* number per group ranged from 3 to 8 mice. For cell experiments, groups included 3–6 replicates. For comparison of two groups, we analyzed data by unpaired *t* test. For comparison of multiple groups at a single time point, we analyzed with ANOVA and Tukey or Sidak's post-test comparison to determine significant differences between groups. For myograph data, groups were analyzed by two-way ANOVA with Tukey post-test comparison at each methacholine dose, to determine significant differences between groups. We used GraphPad Prisms (v8.4.3) to do the statistical analysis. $P < 0.05$ was considered statistically significant.

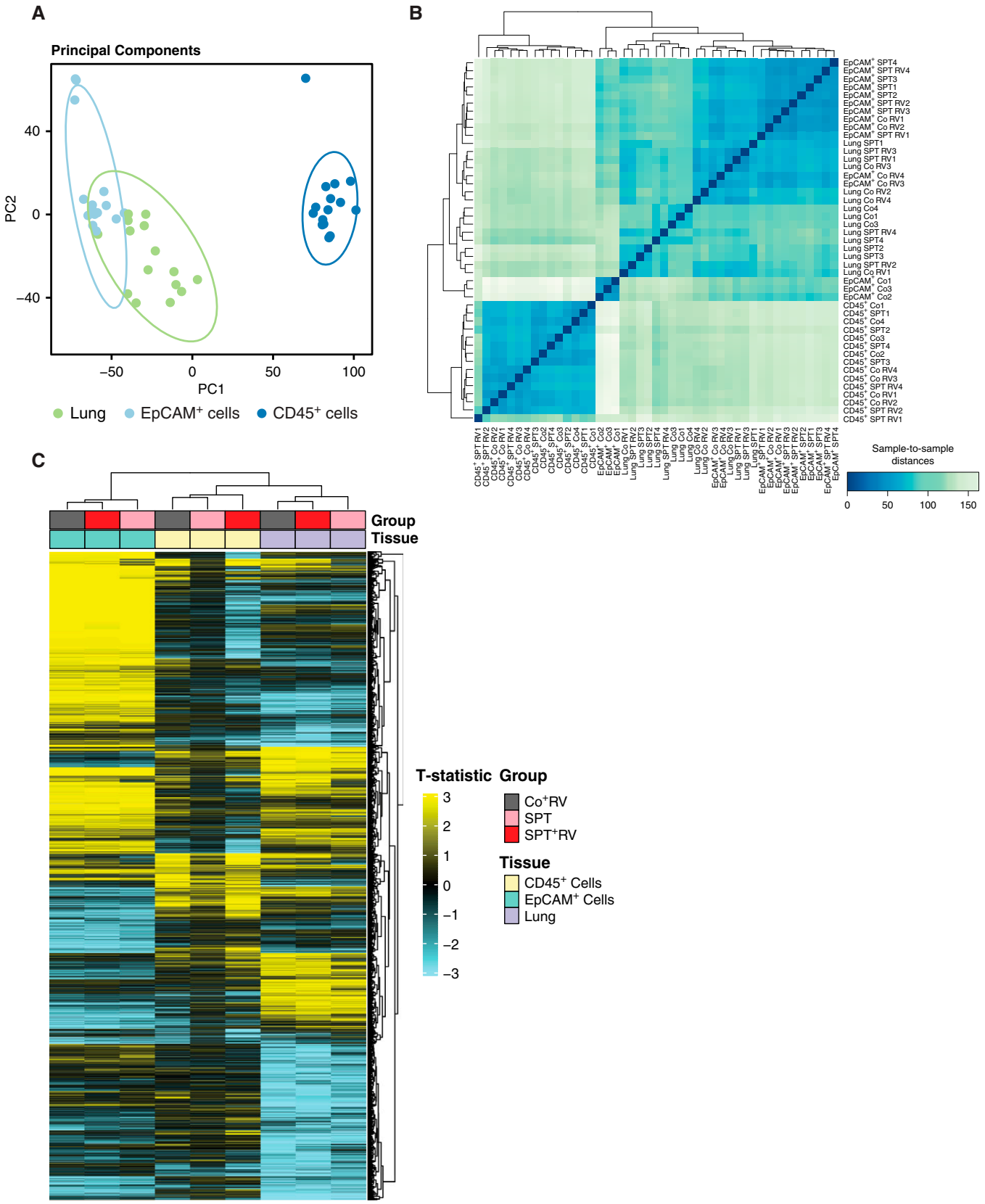

Figure 1. Clustering of lung and lung epithelial transcriptomes from sphingolipid-deficient and rhinovirus (RV)-infected mice. Serine-palmitoyl transferase (SPT) and control (Co) littermates were intranasally inoculated with RV-A1B (5×10^6 Tissue Culture Infectious Dose

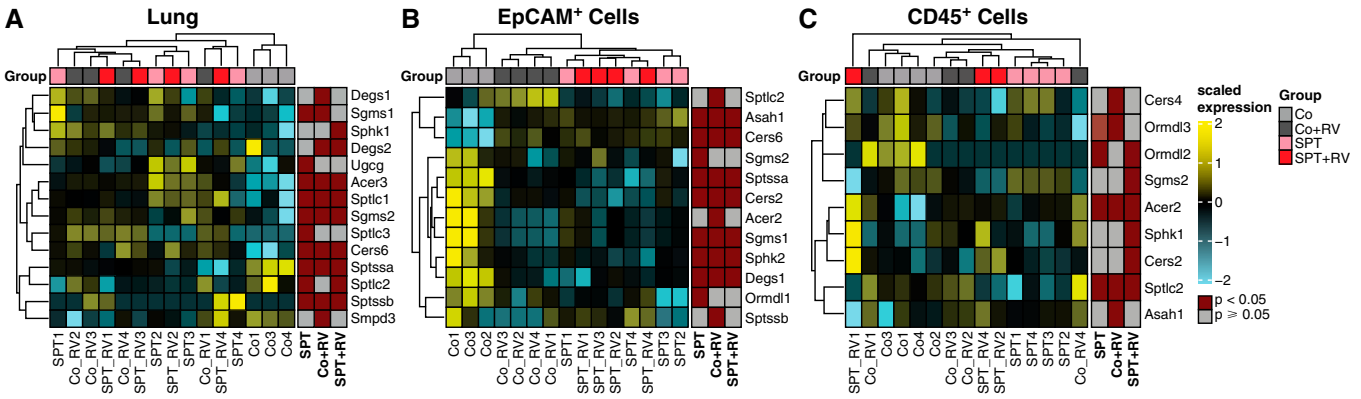

Figure 2. RV infection and SPT deficiency induce similar changes in lung epithelial gene expression for sphingolipid synthesis. Gene ontology enrichment analysis of differentially expressed genes within the sphingolipid synthesis pathway (GO:0030148) for (*A*) lung, (*B*) lung EpCAM$^+$ cells, and (*C*) lung CD45$^+$ cells. Shown are results of hierarchical clustering of differentially expressed genes of Co + RV, SPT, and SPT + RV versus Co mice, with nominal *P* value less than 0.05. Data represent four mice per group for all groups, except those removed after not meeting quality control standards, including one Co sample in the lung and EpCAM$^+$ cell analyses and one SPT + RV sample in the CD45$^+$ analyses.

Results

SPT-Deficiency and RV infection induce correlative gene expression changes

RNA sequencing analysis of lung, lung EpCAM$^+$ cells, and lung CD45$^+$ cells from Co, SPT, Co + RV, and SPT + RV mice showed clustering of sample transcriptomes by cell and tissue type (Figure 1A). This was further illustrated by Pearson correlation analysis, which showed aggregation of lung and lung EpCAM$^+$ cells away from lung CD45$^+$ cells (Figure 1B). Group comparisons of global differential gene expression (DEG) between groups (Co vs. Co + RV, Co vs. SPT, and Co vs. SPT + RV) showed similar expression patterns in lung (Figure 1C, purple) and lung EpCAM$^+$ cells (Figure 1C, teal), but not lung CD45$^+$ cells (Figure 1C, yellow). RV RNA was only present in RV-infected samples and aligned only with the Humanrhinovirus1B_D00239 sequence (Figure E1). No other virus sequences were detected. This suggests that rhinovirus exerts differential effects on the transcriptome of lung epithelial cells and lung CD45$^+$ immune cells.

In comparison with Co mice, KEGG pathway analysis revealed significant overlap in the upregulated (Figure E2A) and downregulated (Figure E2B) pathways of lung EpCAM$^+$ cells from Co + RV and SPT mice. Interestingly, the "sphingolipid signaling" and "protein processing in the endoplasmic reticulum pathways" were upregulated in lung EpCAM$^+$ cells of Co + RV and SPT mice. Additional gene ontology analysis of genes specific to the *de novo* sphingolipid synthesis pathway (29) showed clustering of SPT, Co + RV, and SPT + RV apart from Co mice in the lung (Figure 2A) and lung EPCAM$^+$ cells (Figure 2B), but not lung CD45$^+$ cells (Figure 2C). In both Co + RV and SPT mice, the *de novo* synthesis pathway was upregulated in lung (Figure 2A) and downregulated in lung EpCAM$^+$ cells (Figure 2B). These findings suggest RV infection shifts sphingolipid gene expression to a pattern like SPT inhibition, though with diverging effects in lung and lung epithelial cells.

Next, we analyzed UPR gene expression, as overexpression of ORMDL3 has been shown to activate this pathway (12, 13). Similar to the sphingolipid synthesis genes, UPR gene expression in the lungs (Figure E3A) and lung EpCAM$^+$ cells (Figure E3B) clustered SPT, Co + RV, and SPT + RV together, separate from Co mice. This clustering was not present in lung CD45$^+$ cells (Figure E3C). This suggests RV and genetic inhibition of SPT similarly upregulate the lung UPR stress response primarily in lung epithelial cells.

The type 1 IFN pathway (T1IFN), typically induced by RV infection (30), was upregulated in both Co + RV and SPT + RV mouse tissues (Figure E3). T1IFN gene expression was similar in lung CD45$^+$ cells from Co + RV and SPT + RV mice (Figure E3F). In contrast to the sphingolipid synthesis and UPR pathways, SPT inhibition does not appear to alter T1IFN gene expression at rest or in response to RV infection.

In the lung, top DEGs within the *de novo* sphingolipid synthesis pathway included *Sptssa* and ceramide synthases 2 and 6 (*Cers2* and *Cers6*, respectively). Relative to Co, Sptssa expression was lower in Co + RV and SPT mouse lung (Figure 3A) and lung EpCAM$^+$ cells (Figure 3B). Sptssa expression was similar in SPT and SPT + RV samples. Sptssa expression was similar in lung CD45$^+$ cells for all groups (Figure 3C). Similarly, in lung (Figure 3D) and lung EpCAM$^+$ cells (Figure 3E) Cers2 expression was lower in Co + RV and SPT mouse relative to Co, though differential expression was only significant in lung EpCAM$^+$ cells. Cers2 expression was similar in lung CD45$^+$ cells for all groups

Figure 1. (*Continued*). 50 assay [$TCID_{50}$]/mouse) or equal volumes of mock-infected purified cell lysates. Lungs were harvested 24 hours after infection. Using magnetic bead separation, CD45$^+$ cells and CD45$^-$, epithelial cellular adhesion molecule (EpCAM$^+$) cells were isolated from lung single-cell suspension. RNA sequencing was performed on RNA isolated from lung tissue, lung EpCAM$^+$, and lung CD45$^+$ cells. (*A*) Principal component analysis from whole lung, EpCAM$^+$, and CD45$^+$ cells irrespective of RV infection. (*B*) Sample-to-sample distances based on global gene expression of all groups. (*C*) Global differential gene expression (adjusted *P* value < 0.05) according to tissue type. Data represent four mice per group for all groups, except those removed after not meeting quality control standards including one Co sample in the lung and EpCAM$^+$ cell analyses, and one SPT + RV sample in the CD45$^+$ analyses. PC = principal component.

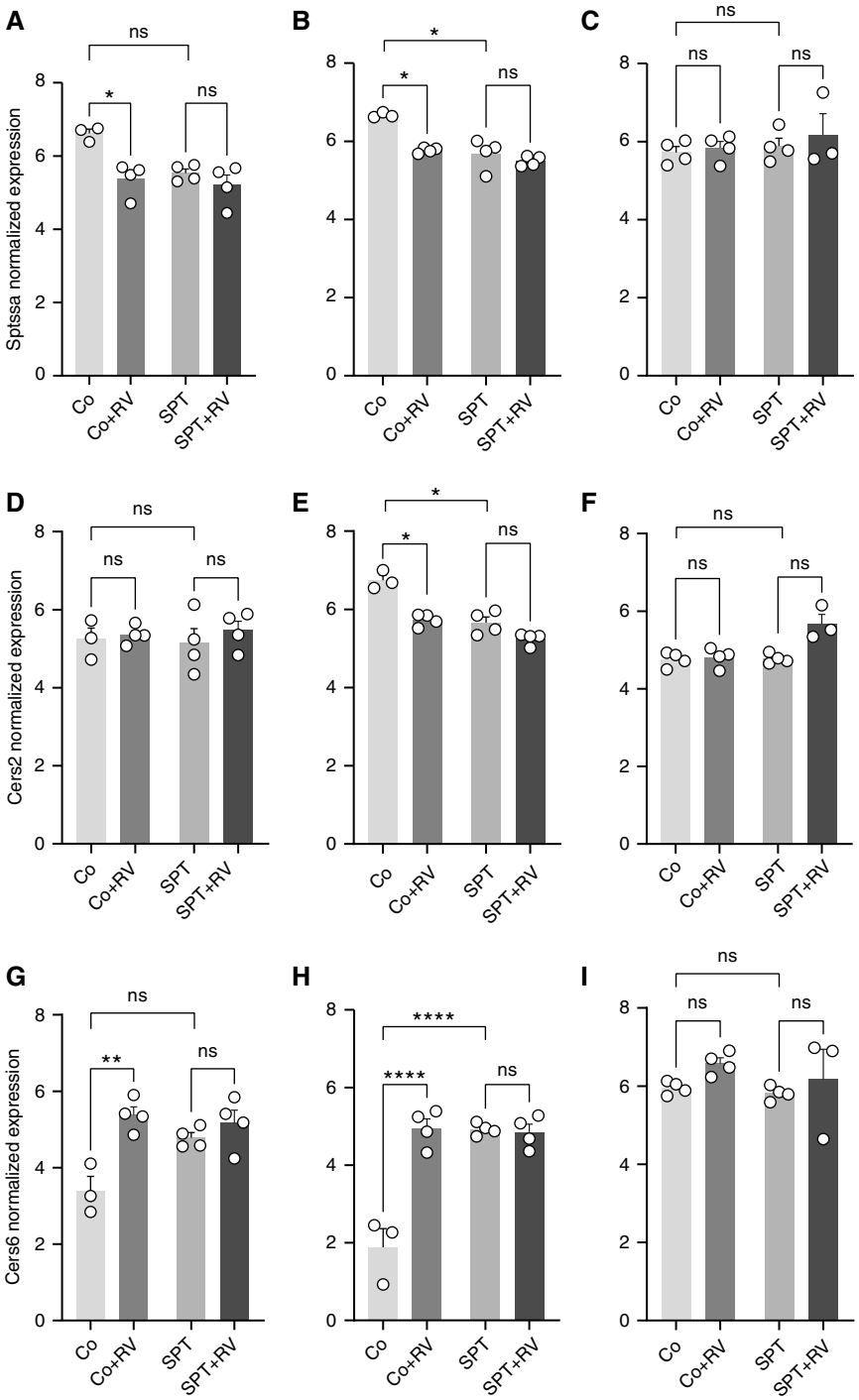

Figure 3. Individual gene analysis following RV infection of wild-type and SPT-deficient lungs and lung epithelial and lung immune cells. In lung, lung EpCAM$^+$ cells, and lung CD45$^+$ cells, normalized expression values of *de novo* sphingolipid genes with differential expression were compared with false discovery threshold adjusted *P* value of 0.05. Normalized expression values calculated using variance-stabilizing transformation. Normalized expression values of Sptssa (small subunit of SPT A) in (*A*) lung, (*B*) lung EpCAM$^+$ cells, and (*C*) lung CD45$^+$ cells. Normalized expression values of Cers2 (ceramide synthase 2) in (*D*) lung, (*E*) lung EpCAM$^+$ cells, and (*F*) lung CD45$^+$ cells. Normalized expression values of Cers6 in (*G*) lung, (*H*) lung EpCAM$^+$ cells, and (*I*) lung CD45$^+$ cells. Shown are means ± SEM of four mice per group for all groups, except those removed after not meeting quality control standards, including one Co sample in the lung and EpCAM$^+$ cell analyses and one SPT + RV sample in the CD45$^+$ analyses. ns = not significant. *$P < 0.05$, **$P < 0.01$, and ****$P < 0.0001$.

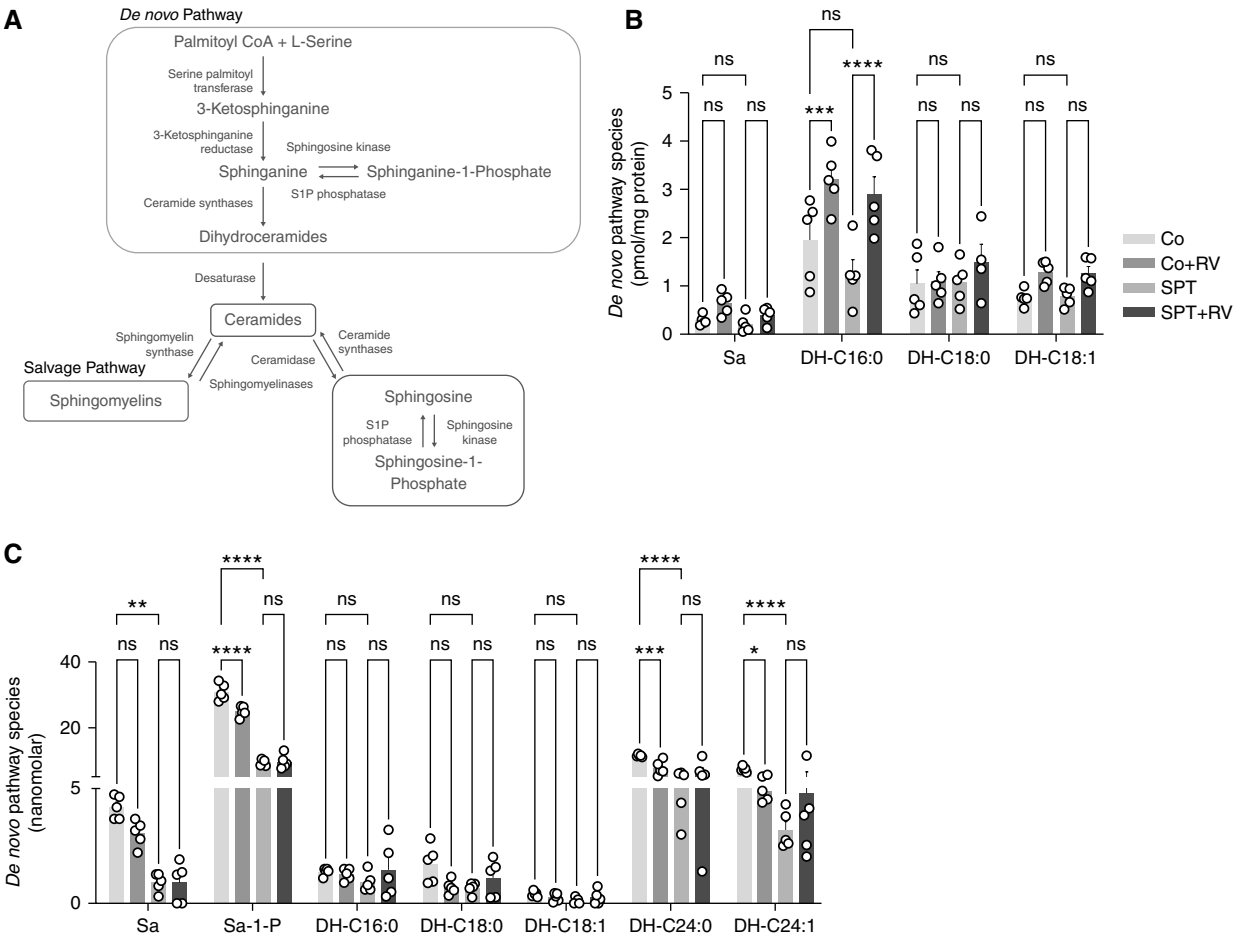

Figure 4. RV infection induces a shift in *de novo* sphingolipid content in lung and blood. (*A*) Sphingolipid synthesis pathways contributing to the synthesis of ceramide metabolites. Blood and perfused, PBS-washed lungs were collected 24 hours after infection and analyzed by HPLC–mass spectrometry (MS)/MS. (*B*) Lung *de novo* synthesis species sphinganine and dihydroceramides C16:0, C18:0, and C18:1. (*C*) Blood *de novo* synthesis species sphinganine, sphinganine-1-phosphate, and dihydroceramides C16:0, C18:0, C18:1, C24:0, and C24:1. Data are representative of two independent experiments with 5–6 mice per group. $^{*}P < 0.05$, $^{**}P < 0.01$, $^{***}P < 0.001$, and $^{****}P < 0.0001$ (two-way ANOVA with Tukey's multiple comparison test). DH = dihydroceramide; S1P = sphinganine-1-phosphate; Sa = sphinganine.

(Figure 3F). In contrast, Cers6 expression was higher in the lungs (Figure 3G) and lung EpCAM$^+$ cells (Figure 3H) of Co + RV and SPT mice compared with Co mice. SPT and SPT + RV mice had similar Cers6 expression. Cers6 expression was similar in lung CD45$^+$ cells for all groups (Figure 3I). This suggests that genetic SPT inhibition and RV similarly affect lung epithelial cell expression of *de novo* sphingolipid synthesis genes, but that these effects are not additive.

Expression of UPR gene Eif2ak2 was increased in the lung (Figure E4A), lung EpCAM$^+$ cells (Figure S4B), and lung CD45$^+$ cells (Figure E4C) of Co + RV and SPT + RV mice, relative to Co and SPT, respectively. SPT mice displayed higher Eif2ak2 expression relative to Co mice (Figure E4A). In lung and all cell types, expression of T1IFN genes Oasl-2 and Cxcl-10 was similar in Co and SPT mice and increased in Co + RV and SPT + RV, respectively (Figure E3). Quantitative PCR analysis confirmed the effects of RV infection on lung and lung EpCAM$^+$ cell expression of *Sptssa, Cers2, Cers6, Eif2ak2, Oasl-2,* and *Cxcl-10* (Figure E5) in Co mice.

RV Infection Induces Shifts in Sphingolipid Content

To assess the effects of RV and SPT deficiency on sphingolipid content, select sphingolipids were quantified in the perfused lung and whole blood of all mice groups by HPLC-MS/MS. This targeted analysis included sphingolipids that are mainly generated through *de novo* synthesis (sphinganine, S1P, and the dihydroceramides [DH], DH-C16:0, DH-C18:0, DH-18:1, DH-C24:0, DH-C24:1); as well as ceramides that can be generated via the *de novo* pathway, salvage pathway, or by hydrolysis of sphingomyelins (Figure 4A) (31). Lung DH-C16:0 was higher in both Co + RV and SPT + RV mice, relative to Co mice (Figure 4B). Relative to Co mice, lung ceramide C24:1 was higher in both Co + RV and SPT + RV (Figure E6A). The ratios of dihydroceramides to sphingomyelins were used to assess relative changes in the *de novo* and salvage pathways. Lung C18:1 dihydroceramide to sphingomyelin (SM) ratio was higher in both Co + RV and SPT + RV, relative to Co mice (Figure E6B). Lung sphingosine levels were similar in all groups (Figure E6C). This suggests that the lung responds to RV infection with increased

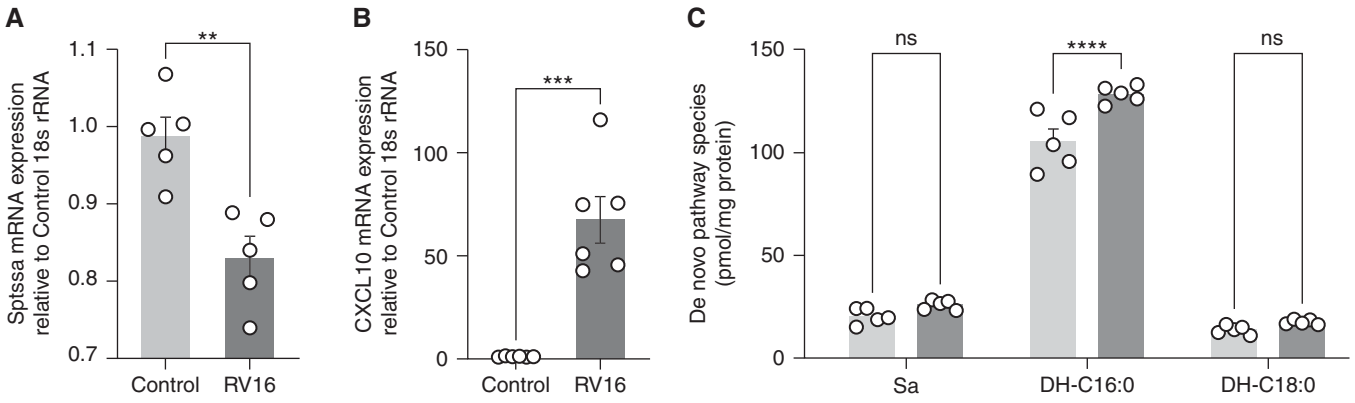

Figure 5. In human bronchial epithelial cells, RV induced similar shifts in gene expression and sphingolipid content in comparison to mouse lung epithelium. BCi NS1.1 cells grown in air–liquid interface were incubated with culture media or RV-A16 (1×10^6 $TCID_{50}$) suspended in culture media for 1 hour at 33°C. After 1 hour, control and infectious media was removed, and incubation continued for 24 hours. Quantitative PCR analysis of mRNA concentrations for genes (*A*) Sptssa and (*B*) Cxcl-10. HPLC-MS/MS measurement of (*C*) *de novo* species sphinganine and DH-C16 and DH-C18. Data are representative of two independent experiments with five samples per group. $^{**}P < 0.01$, $^{***}P < 0.001$, and $^{****}P < 0.0001$. Analyzed by (*A* and *B*) unpaired *t* test and (*C*) two-way ANOVA with Sidak's post-test comparison.

ceramide production, with emphasis on the *de novo* sphingolipid synthesis pathway given the higher concentrations of *de novo* species DH-C16:0, increased DH:SM ratio, and stable sphingosine concentrations.

Relative to Co mice, SPT mice displayed lower blood levels of sphinganine, S1P, DH-C24:0 and DH-C24:1 (Figure 4C), ceramides C22:0, C24:0, C24:1 (Figure E6D), and sphingosine (Figure E6E). Similarly, S1P, DH-C24:0, DH-C24:1 (Figure 4C), ceramide C24:0 (Figure E6D), and sphingosine (Figure E6E) were lower in the blood of Co + RV relative to Co mice. Blood DH:SM ratios were similar among all groups (Figure E6F). This suggests that RV and genetic SPT inhibition similarly reduce blood sphingolipids, including *de novo* sphingolipid species.

RV-1b viral RNA was not detected in the blood of Co + RV mice 24 hours after infection (Figure E7A). Additionally, sphingolipid levels were unchanged in wild-type mouse blood following *ex vivo* infection with RV-1b (Figure E7). This suggests that observed changes in blood sphingolipids following respiratory RV infection do not result from direct interaction between RV and blood cells.

RV Infection Changes Sphingolipid Gene Expression and Sphingolipid Content in Human Bronchial Epithelial Cells

To assess the effect of RV on sphingolipid content and gene expression in human epithelial cells, differentiated human bronchial epithelial cells (BCi-NS1.1) grown in ALI were infected with RV A-16 for 24 hours. As with the murine infections, RV infections decreased expression of Sptssa (Figure 5A) and increased expression of Cxcl-10 (Figure 5B). RV also increased cellular DH-C16:0 (Figure 5C), C18:0 dihydroceramide to sphingomyelin ratio (Figure E8A), and sphingosine (Figure E8B). This suggests the effects of RV on epithelial cell sphingolipids are similar in human and murine airway epithelial cells and following infection with different RV species.

RV Infection Exacerbates SPT-Deficiency-associated Airway Hyperreactivity

Airways of SPT mice are constitutively hyperresponsive in response to methacholine and thus provide a functional model for ORMDL3-associated asthmatic airway hyperreactivity (15, 32). To assess airway reactivity with SPT deficiency and following RV infection, isolated bronchial rings were evaluated in a myograph. Both RV and SPT deficiency increased bronchial ring contractility, independently and then collectively in SPT + RV mice (Figure 6A). BAL neutrophils were also similarly increased in the RV-infected Co and SPT mice (Figure 6B). Lung weight as a percentage of body weight was increased in Co + RV and SPT + RV mice compared with Co and SPT mice 24 hours after infection (Figure 6C). Total white blood cell, neutrophil, and lymphocyte counts were similar in Co and SPT mice before and after infection with RV (Figure 6D). Given the limited effects of RV on the sphingolipid synthesis pathway of $CD45^+$ immune cells, we assessed the dependence of sphingolipid-driven airway reactivity on immune cells by measuring airway reactivity in $RAG^{-/-}$ SPT and $Rag^{-/-}$ Co mice. Interestingly, $Rag^{-/-}$ SPT mice demonstrated increased airway reactivity compared with $Rag^{-/-}$ Co mice (Figure E9A). Following further depletion of innate immune cells with anti-CD90.2, $Rag^{-/-}$, SPT mice maintained an increased airway reactivity compared with $Rag^{-/-}$ Co mice (Figure E9B) (31). Collectively these findings suggest that RV induces airway hyperreactivity and airway neutrophilia within 24 hours, with concurrent changes in lung sphingolipid gene expression and blood sphingolipid content that mimic genetic SPT-deficiency. As the airway hyperreactivity that is associated with reduced SPT activity seems independent of the presence of immune cells, RV-induced airway hyperreactivity may also stem from its effects on the sphingolipid synthesis pathway.

Discussion

Pediatric asthma studies have shown early-life RV-induced wheeze increases the risk of childhood asthma in children with 17q21 asthma risk alleles (21). This association is specific to RV and has not been made with respiratory syncytial virus, another important pathogen in early childhood lung disease. In children with asthma, 17q21

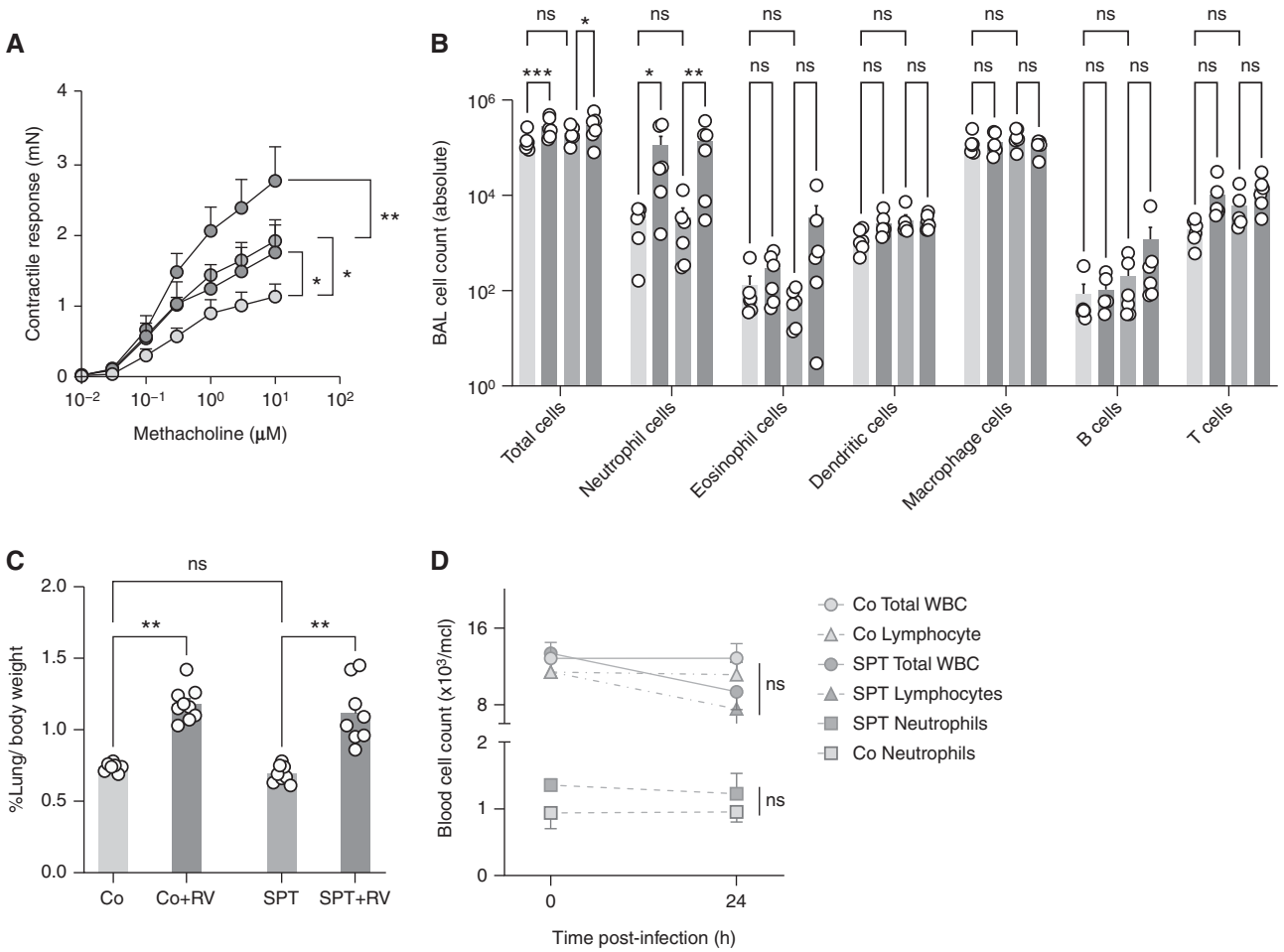

Figure 6. RV infection increases airway reactivity and inflammation in wild-type and SPT-deficient mice. SPT-deficient Sptlc2$^{+/-}$ (SPT) and littermate Co mice were inoculated intranasally with RV-1B (5×10^6 $TCID_{50}$) or mock-infected purified cell lysates. (*A*) Bronchial rings isolated 24 hours after infection were stimulated with increasing doses of methacholine. Shown are contractile responses expressed as the absolute force generated in millinewton (mN). (*B*) BAL cell composition analyzed 24 hours after infection by flow cytometry. (*C*) Relative lung weight 24 hours after infection. (*D*) From blood, total white blood cell count, and manual neutrophil and lymphocyte blood count measured before and after infection from the same mice. Data are means ± SEM or 5–8 animals per group. $^*P < 0.05$, $^{**}P < 0.01$, and $^{***}P < 0.001$ (two-way ANOVA with Tukey post-test comparison). WBC = white blood cells.

asthma risk alleles are now clearly linked to disruptions in sphingolipid *de novo* synthesis (17, 18), likely through overexpression of the SPT inhibitor ORMDL3 (1, 33). Using SPT-deficient Sptlc2$^{+/-}$ heterozygous mice, we investigated the interaction of RV and sphingolipid synthesis in relation to relevant features of asthma. SPT mice have been useful in the study of decreased *de novo* sphingolipid synthesis and asthma, especially as it relates to airway hyperreactivity (15, 32). Alternative 17q21-related models relying on overexpression or knockdown of ORMDL3 or gasdermin B have not shown consistent relation to sphingolipids, likely owing to the stochiometric effects of ORMDL3 on sphingolipid synthesis (34). The SPT-deficient Sptlc2$^{+/-}$ mice have around 40–60% lower tissue sphingolipid concentrations (15, 26) and are thus a good, albeit reductionist, model to study the interaction of asthma-relevant exposures with lower, but not too low, sphingolipid synthesis.

RV is known to increase airway reactivity and airway inflammation within 24 hours of infection (35). Using this time point, we uncovered the complex effects of RV on sphingolipid synthesis. RV shifted lung and lung epithelial cell sphingolipid synthesis gene expression to a pattern that resembled genetic SPT deficiency. Notably, RV reduced gene expression of Sptssa in mouse and human airway epithelial cells. Sptssa is a subunit of SPT that functions to stimulate enzymatic activity, increasing *de novo* synthesis (33, 36). A recent study found Sptssa expression is reduced in the nasal cells of 6-year-old children with asthma and17q21 asthma risk alleles (18), the same alleles linking early-life RV illness and childhood asthma (21). As seen with SPT-deficiency, RV also altered expression of Cers2 and -6. Cers2-null mice similarly display increased Cers6 expression and increased airway resistance (37). RV and genetic deficiency of Sptlc2 appear to confer similar asthma-relevant effects on sphingolipid gene expression.

Concurrent mass spectrometry analysis revealed a complex relationship between gene expression, sphingolipids, and RV infection. RV is known to induce airway epithelial cell production of ceramide-

enriched platforms, which are necessary for viral entry into the cell (38), an effect that may explain increased lung sphingolipids. It is perplexing that both RV infection and genetic SPT inhibition resulted in lung *de novo* gene expression patterns more congruent with sphingolipid concentrations in blood than lung. Studies have shown children with asthma have lower blood dihydroceramides in comparison to those without asthma. Our results suggest RV reduces blood sphingolipid to concentrations like that seen in genetically SPT-deficient mice. The previously mentioned study also found childhood asthma onset correlates with lower plasma S1P concentrations at 6 months of age (18), plausibly before the occurrence of rhinoviral illness. For children with 17q21 asthma risk alleles, early-life RV infection may represent a sentinel event in which existing, gene-induced disturbances of the sphingolipid pathway are durably exacerbated in a "double-hit mechanism". Constitutively lower sphingolipid synthesis may heighten vulnerability to subsequent RV-induced airway hyperreactivity.

Both RV and SPT deficiency increased airway reactivity, with synergistic effect in RV-infected SPT mice. Using Rag-deficient SPT mice, we were able to show the airway effects of SPT deficiency are independent of adaptive immune and innate lymphoid cells but were not able to assess the effects of RV-infection in the immunodeficient mice. The exact mechanisms for the airway reactivity with lower sphingolipid concentrations still need to be elucidated, but recent data suggest that increasing concentrations of sphingolipids within the *de novo* synthesis pathway can alleviate airway hyperreactivity (32). Studies have shown that S1P can directly induce airway contraction (39), but we did not see significant elevations of S1P or sphingosine, its precursor, in RV-infected or SPT mice. Ceramides, including C16:0 and C24:1, have been shown to influence arterial smooth muscle contraction and vascular tone (40, 41). It is not clear if this can be extrapolated to airway smooth muscle. Increased bronchial microvascularity is a component of airway remodeling detectable in children with asthma (42, 43). Lower blood sphingolipids may correlate with bronchial microvessel tone, resulting in early airway remodeling and bronchial hyperresponsiveness. More work is needed to understand the implications of blood sphingolipids on airway vasculature and airway hyperresponsiveness.

SPT deficiency was independently associated with increased UPR gene expression, another pathway influenced by ORMDL3 (19). UPR is important for viral "sensing" and inflammatory cytokine release but can also be manipulated to promote viral replication (44). Here, the T1IFN pathway appears equally upregulated in wild-type and SPT mice. Viral RV RNA counts and BAL cellular composition were similar in both RV-infected wild-type and SPT mice, suggesting the inflammatory/antiviral response to RV was not altered by SPT-deficiency. There is recent evidence that SPT mice display dysfunctional $CD8^+$ T cells and a reduced antiviral response to lymphocytic choriomeningitis virus (LCMV) (45). Our study only assessed responses at 24 hours after infection, a time point unlikely to be affected by CD8 cells (35). However, this may also reflect a limitation to using an SPT mouse model as it remains unclear if and how ORMDL3-related asthma genotypes alter susceptibility to RV infection (21, 46).

Overall, the RV's effects on the sphingolipid pathway offer a point of connection between 17q21 asthma risk alleles, RV-induced wheeze (21), and childhood asthma. Our findings suggest RV can shift sphingolipid metabolism to a pattern of SPT deficiency, an effect that may intensify suboptimal *de novo* synthesis and airway reactivity in children with 17q21 asthma risk alleles. This study elevates the role of *de novo* sphingolipid synthesis in the pathogenesis of asthma and RV-induced asthma exacerbations. ■

Author disclosures are available with the text of this article at www.atsjournals.org.

Acknowledgment: The authors thank Ronay Menschel, Christine and Pasco Alfaro, and Joanna Weiss for their generous support. They also thank X. Chiang for the SPT mice and R. G. Crystal for the human airway epithelial cell line.

References

1. Moffatt MF, Kabesch M, Liang L, Dixon AL, Strachan D, Heath S, *et al.* Genetic variants regulating ORMDL3 expression contribute to the risk of childhood asthma. *Nature* 2007;448:470–473.
2. Loss GJ, Depner M, Hose AJ, Genuneit J, Karvonen AM, Hyvärinen A, *et al.*; PASTURE (Protection against Allergy Study in Rural Environments) Study Group. The early development of wheeze. Environmental determinants and genetic susceptibility at 17q21. *Am J Respir Crit Care Med* 2016;193:889–897.
3. Bisgaard H, Bønnelykke K, Sleiman PM, Brasholt M, Chawes B, Kreiner-Møller E, *et al.* Chromosome 17q21 gene variants are associated with asthma and exacerbations but not atopy in early childhood. *Am J Respir Crit Care Med* 2009;179:179–185.
4. Halapi E, Gudbjartsson DF, Jonsdottir GM, Bjornsdottir US, Thorleifsson G, Helgadottir H, *et al.* A sequence variant on 17q21 is associated with age at onset and severity of asthma. *Eur J Hum Genet* 2010;18:902–908.
5. Moffatt MF, Gut IG, Demenais F, Strachan DP, Bouzigon E, Heath S, *et al.*; GABRIEL Consortium. A large-scale, consortium-based genomewide association study of asthma. *N Engl J Med* 2010;363:1211–1221.
6. Bouzigon E, Corda E, Aschard H, Dizier M-H, Boland A, Bousquet J, *et al.* Effect of 17q21 variants and smoking exposure in early-onset asthma. *N Engl J Med* 2008;359:1985–1994.
7. Davis DL, Gable K, Suemitsu J, Dunn TM, Wattenberg BW. The ORMDL/Orm-serine palmitoyltransferase (SPT) complex is directly regulated by ceramide: reconstitution of SPT regulation in isolated membranes. *J Biol Chem* 2019;294:5146–5156.
8. Han S, Lone MA, Schneiter R, Chang A. Orm1 and Orm2 are conserved endoplasmic reticulum membrane proteins regulating lipid homeostasis and protein quality control. *Proc Natl Acad Sci USA* 2010;107:5851–5856.
9. Siow D, Sunkara M, Morris A, Wattenberg B. Regulation of de novo sphingolipid biosynthesis by the ORMDL proteins and sphingosine kinase-1. *Adv Biol Regul* 2015;57:42–54.
10. Oyeniran C, Sturgill JL, Hait NC, Huang WC, Avni D, Maceyka M, *et al.* Aberrant ORM (yeast)-like protein isoform 3 (ORMDL3) expression dysregulates ceramide homeostasis in cells and ceramide exacerbates allergic asthma in mice. *J Allergy Clin Immunol* 2015;136:1035–46.e6.
11. Breslow DK, Collins SR, Bodenmiller B, Aebersold R, Simons K, Shevchenko A, *et al.* Orm family proteins mediate sphingolipid homeostasis. *Nature* 2010;463:1048–1053.
12. Miller M, Rosenthal P, Beppu A, Gordillo R, Broide DH. Oroscomucoid like protein 3 (ORMDL3) transgenic mice have reduced levels of

sphingolipids including sphingosine-1-phosphate and ceramide. *J Allergy Clin Immunol* 2017;139:1373–1376.e4.
13. Miller M, Tam AB, Cho JY, Doherty TA, Pham A, Khorram N, *et al.* ORMDL3 is an inducible lung epithelial gene regulating metalloproteases, chemokines, OAS, and ATF6. *Proc Natl Acad Sci USA* 2012;109:16648–16653.
14. Miller M, Tam AB, Mueller JL, Rosenthal P, Beppu A, Gordillo R, *et al.* Cutting edge: targeting epithelial ORMDL3 increases, rather than reduces, airway responsiveness and is associated with increased sphingosine-1-phosphate. *J Immunol* 2017;198:3017–3022.
15. Worgall TS, Veerappan A, Sung B, Kim BI, Weiner E, Bholah R, *et al.* Impaired sphingolipid synthesis in the respiratory tract induces airway hyperreactivity. *Sci Transl Med* 2013;5:186ra67.
16. Edukulla R, Rehn K, Lindsley AW. Depletion of sphingolipids in a murine model of allergic asthma exacerbates airway hyper responsiveness by increasing Th2 cells. *Am J Respir Crit Care Med* 2015;191:A6436.
17. Ono JG, Kim BI, Zhao Y, Christos PJ, Tesfaigzi Y, Worgall TS, *et al.* Decreased sphingolipid synthesis in children with 17q21 asthma-risk genotypes. *J Clin Invest* 2020;130:921–926.
18. Rago D, Pedersen CT, Huang M, Kelly RS, Gürdeniz G, Brustad N, *et al.* Characteristics and mechanisms of a sphingolipid-associated childhood asthma endotype. *Am J Respir Crit Care Med* 2021;203:853–863.
19. Cantero-Recasens G, Fandos C, Rubio-Moscardo F, Valverde MA, Vicente R. The asthma-associated ORMDL3 gene product regulates endoplasmic reticulum-mediated calcium signaling and cellular stress. *Hum Mol Genet* 2010;19:111–121.
20. Sykes A, Johnston SL. Etiology of asthma exacerbations. *J Allergy Clin Immunol* 2008;122:685–688.
21. Calışkan M, Bochkov YA, Kreiner-Møller E, Bønnelykke K, Stein MM, Du G, *et al.* Rhinovirus wheezing illness and genetic risk of childhood-onset asthma. *N Engl J Med* 2013;368:1398–1407.
22. Cox DW, Khoo S-K, Zhang G, Lindsay K, Keil AD, Knight G, *et al.* Rhinovirus is the most common virus and rhinovirus-C is the most common species in paediatric intensive care respiratory admissions. *Eur Respir J* 2018;52:1800207.
23. Grassmé H, Riehle A, Wilker B, Gulbins E. Rhinoviruses infect human epithelial cells via ceramide-enriched membrane platforms. *J Biol Chem* 2005;280:26256–26262.
24. Zhang Y, Willis-Owen SAG, Spiegel S, Lloyd CM, Moffatt MF, Cookson WOCM. The ORMDL3 asthma gene regulates ICAM1 and has multiple effects on cellular inflammation. *Am J Respir Crit Care Med* 2019;199: 478–488.
25. Liu Y, Bochkov YA, Eickhoff JC, Hu T, Zumwalde NA, Tan JW, *et al.* Orosomucoid-like 3 supports rhinovirus replication in human epithelial cells. *Am J Respir Cell Mol Biol* 2020;62:783–792.
26. Hojjati MR, Li Z, Jiang XC. Serine palmitoyl-CoA transferase (SPT) deficiency and sphingolipid levels in mice. *Biochim Biophys Acta* 2005; 1737:44–51.
27. Wang W, Lee WM, Mosser AG, Rueckert RR. WIN 52035-dependent human rhinovirus 16: assembly deficiency caused by mutations near the canyon surface. *J Virol* 1998;72:1210–1218.
28. Wang G, Lou HH, Salit J, Leopold PL, Driscoll S, Schymeinsky J, *et al.* Characterization of an immortalized human small airway basal stem/progenitor cell line with airway region-specific differentiation capacity. *Respir Res* 2019;20:196.
29. Gault CR, Obeid LM, Hannun YA. An overview of sphingolipid metabolism: from synthesis to breakdown. *Adv Exp Med Biol* 2010; 688:1–23.
30. Bartlett NW, Slater L, Glanville N, Haas JJ, Caramori G, Casolari P, *et al.* Defining critical roles for NF-κB p65 and type I interferon in innate immunity to rhinovirus. *EMBO Mol Med* 2012;4:1244–1260.
31. Sonnenberg GF, Monticelli LA, Alenghat T, Fung TC, Hutnick NA, Kunisawa J, *et al.* Innate lymphoid cells promote anatomical containment of lymphoid-resident commensal bacteria. *Science* 2012; 336:1321–1325.
32. Heras AF, Veerappan A, Silver RB, Emala CW, Worgall TS, Perez-Zoghbi J, *et al.* Increasing sphingolipid synthesis alleviates airway hyperreactivity. *Am J Respir Cell Mol Biol* 2020;63:690–698.
33. Li S, Xie T, Liu P, Wang L, Gong X. Structural insights into the assembly and substrate selectivity of human SPT-ORMDL3 complex. *Nat Struct Mol Biol* 2021;28:249–257.
34. Siow D, Sunkara M, Dunn TM, Morris AJ, Wattenberg B. ORMDL/serine palmitoyltransferase stoichiometry determines effects of ORMDL3 expression on sphingolipid biosynthesis. *J Lipid Res* 2015;56:898–908.
35. Bartlett NW, Walton RP, Edwards MR, Aniscenko J, Caramori G, Zhu J, *et al.* Mouse models of rhinovirus-induced disease and exacerbation of allergic airway inflammation. *Nat Med* 2008;14:199–204.
36. Han G, Gupta SD, Gable K, Niranjanakumari S, Moitra P, Eichler F, *et al.* Identification of small subunits of mammalian serine palmitoyltransferase that confer distinct acyl-CoA substrate specificities. *Proc Natl Acad Sci USA* 2009;106:8186–8191.
37. Petrache I, Kamocki K, Poirier C, Pewzner-Jung Y, Laviad EL, Schweitzer KS, *et al.* Ceramide synthases expression and role of ceramide synthase-2 in the lung: insight from human lung cells and mouse models. *PLoS One* 2013;8:e62968.
38. Cazzaniga M, Varricchio C, Montefrancesco C, Feroce I, Guerrieri-Gonzaga A. Fenretinide (4-HPR): a preventive chance for women at genetic and familial risk? *J Biomed Biotechnol* 2012;2012: 172897.
39. Ammit AJ, Hastie AT, Edsall LC, Hoffman RK, Amrani Y, Krymskaya VP, *et al.* Sphingosine 1-phosphate modulates human airway smooth muscle cell functions that promote inflammation and airway remodeling in asthma. *FASEB J* 2001;15:1212–1214.
40. Cantalupo A, Sasset L, Gargiulo A, Rubinelli L, Del Gaudio I, Benvenuto D, *et al.* Endothelial sphingolipid de novo synthesis controls blood pressure by regulating signal transduction and NO via ceramide. *Hypertension* 2020;75:1279–1288.
41. Zheng T, Li W, Wang J, Altura BT, Altura BM. Sphingomyelinase and ceramide analogs induce contraction and rises in [Ca(2+)](i) in canine cerebral vascular muscle. *Am J Physiol Heart Circ Physiol* 2000;278: H1421–H1428.
42. Barbato A, Turato G, Baraldo S, Bazzan E, Calabrese F, Panizzolo C, *et al.* Epithelial damage and angiogenesis in the airways of children with asthma. *Am J Respir Crit Care Med* 2006;174:975–981.
43. Zanini A, Chetta A, Imperatori AS, Spanevello A, Olivieri D. The role of the bronchial microvasculature in the airway remodelling in asthma and COPD. *Respir Res* 2010;11:132.
44. Smith JA. A new paradigm: innate immune sensing of viruses via the unfolded protein response. *Front Microbiol* 2014;5:222.
45. Wu J, Ma S, Sandhoff R, Ming Y, Hotz-Wagenblatt A, Timmerman V, *et al.* Loss of neurological disease HSAN-I-associated gene SPTLC2 impairs $CD8^+$ T cell responses to infection by inhibiting T cell metabolic fitness. *Immunity* 2019;50:1218–1231.e5.
46. Read JF, Bosco A. Decoding susceptibility to respiratory viral infections and asthma inception in children. *Int J Mol Sci* 2020;21:6372.